EasyChair Preprint

№ 7104

Numerical Study for Flow Behavior and Drag of Axisymmetric Boattail Models at Different Mach Number

The Hung Tran, Cong Truong Dao, Dinh Anh Le and Trang Minh Nguyen

November 28, 2021

Numerical study for flow behavior and drag of axisymmetric boattail models at different Mach number

The Hung Tran [1*], Cong Truong Dao[2], Dinh Anh Le[3], Tran Minh Nguyen[4]

[1] *Faculty of Aerospace Engineering, Le Quy Don Technical University, Hanoi, Vietnam*

[2] *Co-first author, PhD student, Academy of Military Science Technology, Hanoi, Vietnam*

[3] *School of Aerospace Engineering, University of Engineering and Technology, National University (Hanoi), Hanoi, Vietnam*

[4] *Academy of Military Science Technology, Hanoi, Vietnam*

* Corresponding author: *tranthehung_k24@lqdtu.edu.vn*

Abstract

In this study, flow behavior around an axisymmetric boattail model was presented at different Mach number from subsonic to supersonic flow. Reynolds averaged Navier-Stokes equations with k-ω SST model was applied for the simulation. Results were validated with previous relevant experimental data for validation. The results indicated that the numerical model can provide high accurate results. The different in drag coefficients of the current and relevant studies is less than 3%. Pressure distribution showed that at supersonic flow, pressure becomes nearly flat on the boattail surface due to generation of shock wave. Skin-friction indicated separation bubble is formed only for low-speed conditions at boattail angle of 14°. At higher Mach number, separation positions occurred at the base edge for all models and flow conditions. The pressure trend, position of shock wave, and flow pattern around the model was indicated details in this study. The relation between shock-wave structure and drag of the model was obtained.

Keywords: axisymmetric boattail, shock wave, separation flow, skin friction

1 Introduction

In engineering, many flying objects were designed with blunt base such as missibles or projectile. The design is satisfied for insert engine or initial lauching conditions. However, the blunt base model forms a large wake during the flight, which results in increasing drag and reduce aerodynamic performance.

The methods to reducing wake structure includes active and passive devices . Active methods, which include external burning or base bleed, provide a significant power source to eliminate the wake [1]. However, the design of active control device is quickly complicated and it is suitable for missible only during the working state of engine. In constract, the passive devices reduce intensity of the wake by modified the base configuration. The candidate of passive devices includes backward step, locked-vortex afterbody, cavity and boattail geometry [2]–[5]. The boattail is seemingly a high effective method for reduce the drag and it has been applied widely in engineering.

Previous studies for boattail model were conducted by Platou et al. [6], Visnawath et al.[7][8], Tran et al. [9] and the others. The optimization configuration, which showed minimum drag level at supersonic flow, has angle of around 7° and the boattail length of around one diameter. For low-speed flow, Tran et al. indicated that the optimization angle was much higher than the case of supersonic conditions. Exception of many studies, previous investigations focured only drag of the model. The relation between flow fields and drag reduction was not taken attention.

The limiation of previous studies was probably linked with the cost of experiments in supersonic flow. In fact, experimental study is quitely expensive and devices for the measurement are limited. In fact, only some parameter can be measured for different experiments. Additionally, time for measurement at supersonic flow is ofter short. Consequently, it is challenge for obtaining all parameters in some limited measurements.

Presently, the development of computational technology provide a tool for analyzing aerodynamic characteristics of the moving vehicles. The finite volume methods are applied to solve Navier-Stokes equations, which could provide different accurate level of the flow fields. In fact, combining with experimental results, numerical methods could extend study and provide prediction of the aerodynamic phenomenon. In fact, numerical methods have been widely applied in previous studies for analyzing flow behavior and drag of boattail model [10]–[12].

In this study, the flow behavior around axisymmetic boattail models was investigated at different free-stream conditions. We focus on two conical boattail angle of 7° and 14° for the investigation. The two models are featured for optimization drag at supersonic and subsonic

conditions. Reynolds averaged Navier-Stokes (RANS) equations with *k-ω* SST model was applied for analyzing flow fields and drag. The numerical setup and validation methods are presented in section 2 of this study. Next, section 3 shows the results of this study. Finally, the paper is conclused in section 4.

2 Numerical setup and validations

2.1 Numerical model

For numerical simulation, we use the same model as it was presented in previous study by Platou et al. [6]. The diameter *D* of the model is 57 mm and its total length is 228 mm. The model has elliptical shape of the nose and cylinder part for the main body. The boattail part has conical shape with fixed length of 1*D*. The shape of the model is indicated in Fig. 1. Two conical boattail angles of 7° and 14° were used in this study. Note that two models of 7° and 14° are optimization boattail angles for flow at subsonic and supersonic conditions, respectively.

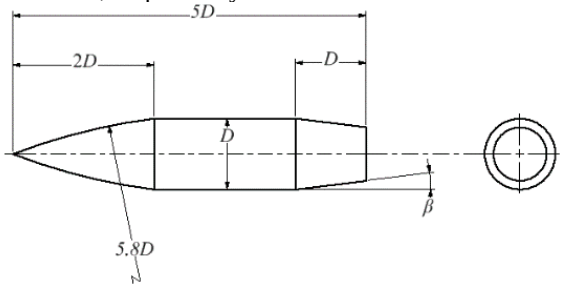

Fig. 1. Model geometry

2.2 Numerical algorithm

In this study, RANS equations with *k-ω* SST turbulence model is applied for the simulation. To obtain the RANS equations, averaged filters are applied to Navier-Stokes equations, which contain continuous equation, three momentum equations and the energy equation. As the results, only averaged flow fields can be obtained. The *k-ω* SST turbulence model contains two additional equations for simulation of turbulent characteristics [13]. The model allows to obtain high accurate results near the model surface and reduce the numerical time. The Navier-Stockes equations are shown as:

$$\frac{\partial \rho}{\partial t} + \mathrm{div}(\rho U) = 0 \tag{1}$$

$$\begin{aligned}
&\frac{\partial(\rho u)}{\partial t} + \frac{\partial(\rho u^2)}{\partial x} + \frac{\partial(\rho uv)}{\partial y} + \frac{\partial(\rho uw)}{\partial z} = \\
&= -\frac{\partial p}{\partial x} + \frac{\partial}{\partial x}\left(\lambda \nabla.U + 2\mu \frac{\partial u}{\partial x}\right) + \frac{\partial}{\partial y}\left[\mu\left(\frac{\partial v}{\partial x} + \frac{\partial u}{\partial y}\right)\right] + \frac{\partial}{\partial z}\left[\mu\left(\frac{\partial v}{\partial z} + \frac{\partial u}{\partial x}\right)\right] \\
&\frac{\partial(\rho v)}{\partial t} + \frac{\partial(\rho uv)}{\partial x} + \frac{\partial(\rho v^2)}{\partial y} + \frac{\partial(\rho vw)}{\partial z} = \\
&= -\frac{\partial p}{\partial y} + \frac{\partial}{\partial x}\left[\mu\left(\frac{\partial v}{\partial x} + \frac{\partial u}{\partial y}\right)\right] + \frac{\partial}{\partial y}\left(\lambda \nabla.U + 2\mu \frac{\partial v}{\partial x}\right) + \frac{\partial}{\partial z}\left[\mu\left(\frac{\partial w}{\partial y} + \frac{\partial v}{\partial z}\right)\right] \\
&\frac{\partial(\rho w)}{\partial t} + \frac{\partial(\rho uv)}{\partial x} + \frac{\partial(\rho vw)}{\partial y} + \frac{\partial(\rho w^2)}{\partial z} = \\
&= -\frac{\partial p}{\partial z} + \frac{\partial}{\partial x}\left[\mu\left(\frac{\partial v}{\partial z} + \frac{\partial w}{\partial x}\right)\right] + \frac{\partial}{\partial y}\left[\mu\left(\frac{\partial w}{\partial y} + \frac{\partial v}{\partial z}\right)\right] + \frac{\partial}{\partial z}\left(\lambda \nabla.U + 2\mu \frac{\partial w}{\partial z}\right) \\
&\frac{\partial}{\partial t}\left[\rho\left(e + \frac{U^2}{2}\right)\right] + \nabla\left[\rho\left(e + \frac{U^2}{2}\right)\right] = \rho\dot{q} - \frac{\partial}{\partial x}\left(k\frac{\partial T}{\partial x}\right) + \frac{\partial}{\partial y}\left(k\frac{\partial T}{\partial y}\right) \\
&+ \frac{\partial}{\partial z}\left(k\frac{\partial T}{\partial z}\right) - p\left(\frac{\partial u}{\partial x} + \frac{\partial v}{\partial y} + \frac{\partial w}{\partial z}\right) + \frac{\partial(u\tau_{xx})}{\partial x} + \frac{\partial(u\tau_{yx})}{\partial y} + \frac{\partial(u\tau_{zx})}{\partial z} \\
&+ \frac{\partial(v\tau_{xy})}{\partial x} + \frac{\partial(v\tau_{yy})}{\partial y} + \frac{\partial(v\tau_{zy})}{\partial z} + \frac{\partial(w\tau_{xz})}{\partial x} + \frac{\partial(w\tau_{yz})}{\partial y} + \frac{\partial(w\tau_{zz})}{\partial z}
\end{aligned} \tag{3}$$

where $U = (u, v, w)$ is velocity vector, p is pressure ρ is air density, μ is viscosity and $\lambda = -2/3\mu$.τ_{ij} is stress tensor of component i, j, T is temperature. The first equation shows the equation of the mass conservation, the next three equations are momentum equations and the last equation is the energy equation. For steady flow, derivative of functions with time is zero, which allows to reduce parameters and numerical time in those equation. The two additional equations for k and ω are written as:

$$\begin{aligned}
&\frac{\partial(\rho k)}{\partial t} + \frac{\partial(\rho u_j k)}{\partial x_j} = P = \beta^* \rho\omega k + \frac{\partial}{\partial x_j}\left[(\mu + \sigma_k \mu_t)\frac{\partial k}{\partial x_j}\right] \\
&\frac{\partial(\rho\omega)}{\partial t} + \frac{\partial(\rho u_j \omega)}{\partial x_j} = \frac{\gamma}{\nu_t} P - \beta\rho\omega^2 + \frac{\partial}{\partial x_j}\left[(\mu + \sigma_k \mu_t)\frac{\partial \omega}{\partial x_j}\right] \\
&+2(1 - F_1)\frac{\rho\sigma_{\omega 2}}{\omega}\frac{\partial k}{\partial x_j}\frac{\partial \omega}{\partial x_j}
\end{aligned} \tag{4}$$

Where ν_t is eddy-viscosity and is defined as:

$$\nu_t = \frac{a_1 k}{\max(a_1\omega; \Omega F_2)} \tag{5}$$

and σ_k, $\sigma_{\omega 2}$, β, β^*, κ, γ are constant parameters. The criteria for selecting those numbers were presented in previous studies by Menter. The model was applied in our previous study and showed good performance in analyzing boattail flow.

In this study, we use comercial software Ansys Fluent Version 21.1, which was copyrighted by Le Quy Don Technical university for the simulation. The dicrete of the deviative were selected as second order of accuracy. SIMPLE algorithm was selected for velocity vectors and pressure fields. Other parameters are then intergrated from the velocity and pressure. Depending on flow conditions, different inlet stratery was selected. The residual of the numerical scheme is less than 10^{-5}.

2.3 Mesh generation

The structure mesh is applied in this study for numerical simulation. Mesh around the model is indicated in Fig. 2. The thickness of the first layer is 2×10^{-7}m and the increasing ratio is 1.15. The $y^+<1$ for all the numerical cases.

Numerical domain has a dimension of 36.5 D × 22 D × 22 D in x, y and z directions. In subsonic conditions, velocity inlet is selected for the inlet flow. The pressure far fields is selected for supersonic

conditions. The outlets are setup as pressure outlet for both subsonic and supersonic conditions.

To check the grid cell independence, mesh size from 1.44 million cells to 4.40 million cells is selected. The dependence of drag on volume of the mesh is indicated in Table 1. Here, drag coefficient is calcuated based on maximum cross-section area of the model. It shows that when the number of cells exceeds 3.16 million, the drag becomes nearly constant. Consequently, mesh size with 3.16 million cells are selected for this study. Note that previous study indiated that the number of mesh size above 2.6 million cells are sufficient for boattail investigation [10].

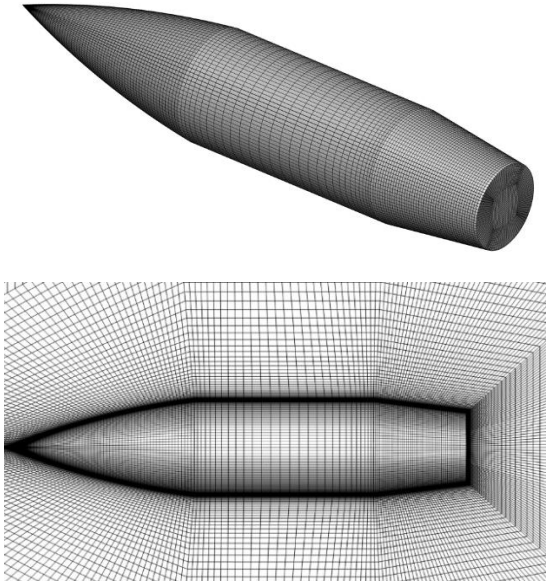

Fig. 2. Mesh around the models

Mesh size (Mil. Cells)	1.45	2.35	3.16	3.88	4.37
C_D	0.323	0.320	0.318	0.318	0.318

Table 1. Drag as function of mesh size

3 Results and discussion

3.1 Validations

To validate the results, we compare drag coefficient of the current study with experimental results by Platou at supersonic flow for boattail angle of 7°. The results of different methods are shown in Fig. 3. Results using *k-ε* turbulence model by Elawwad [10] also indicated. Clearly, at supersonic flow, trend of drag is similar for three numerical methods. The difference of drag coefficient of the current and previous study is less than 3°. It is explained that the method in this study allows to obtain high accurate results of drag on the model. The numerical methods can be applied for extended the study.

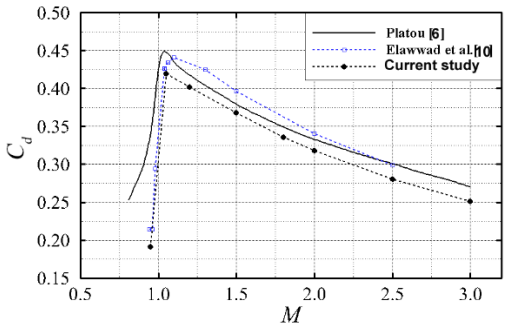

Fig. 3. Drag coefficient by different methods

3.2 Pressure distribution on boattail surface

Figure 4 shows distribution of pressure coefficients around the model for Mach number of M = 3.0. Clearly, numerical results allow to full picture of pressure distribution on the surface and other parameters. The model is feature by high pressure in the nose region. On the boattail surface, pressure becomes nearly constant for M = 3.0. Since the front and main parts are similar for all configuration, pressure distributions on boattail and base surface will be focused to explain drag trend of the model.

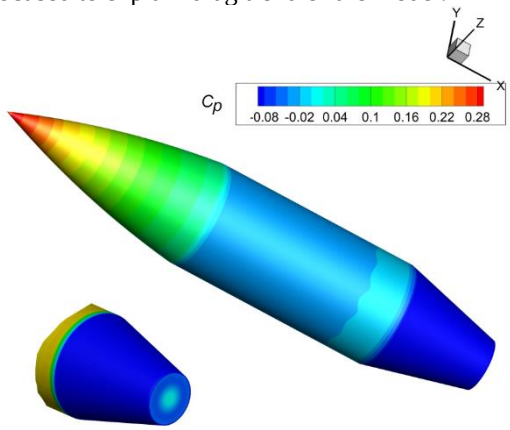

Fig. 4. Pressure coefficient around the model at M = 3

Pressure distribution on the boattail and base surfaces are shown in Fig. 5, and Fig. 6 for the angle of 7° and 14°, respectively. For the base surface, the *D'* presents the diameter of the base. Interestingly, pressure gradient becomes higher with increasing Mach number in subsonic conditions. In the second half of the model, pressure receovery is similar for both flow conditions. At supersonic flow, pressure becomes nearly flat, which is caused by formalization of shock wave on the surface. The negative pressure leads to inceasing total drag of the model.

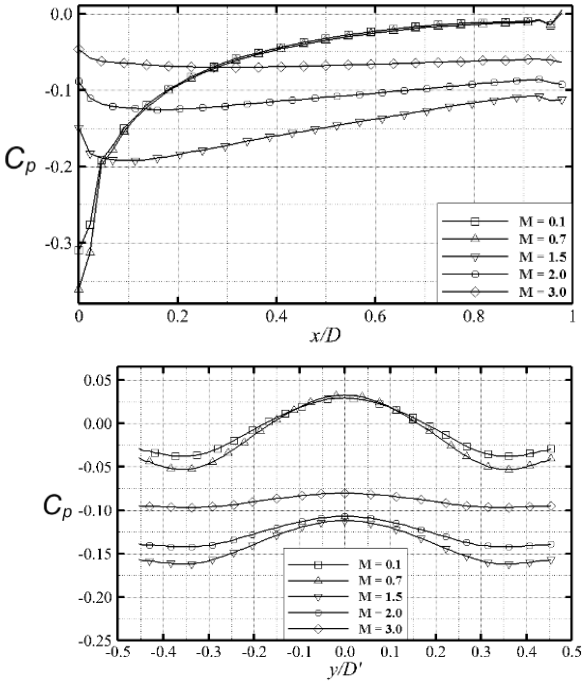

Fig. 5. Pressure distribution boattail (top) and base (bottom) surfaces at β = 7°

Figure 5b shows pressure distribution on the base for boattail model of 7°. For all Mach number, the tendency of pressure is similar with a maximum values near at the center of the model. The trend of pressure distribution also shows that base drag of the model at supersonic flow is much higher than the case of subsonic flow. For boattail model of 14°, similar trend of pressure on boattail and base surfaces is obtained (Fig. 6).

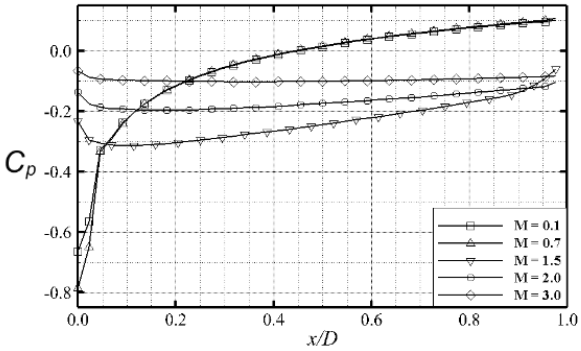

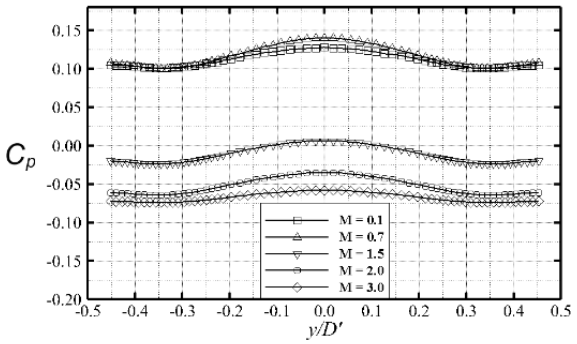

Fig. 6. Pressure distribution boattail (top) and base (bottom) surfaces at β = 14°

Figures 7 and 8 illustrate the contour of Mach number around the model for the angle of 7° and 14°, respectively. Similar Mach contour is observed for both cases. Here, a large shock wave occurs at the nose of the model. On the boattail region, the Mach number is higher than free-stream Mach number, which is caused the change of boundary layer profile and the existence of shock-wave. It should be note that the main difference of the flow at subsonic and supersonic conditions is from the shock wave on the base surface.

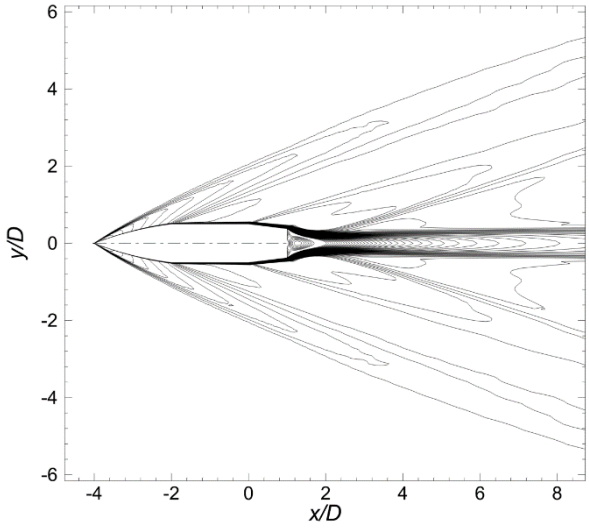

Fig. 7. Mach numer countor around the model at β = 7° and M = 3.0

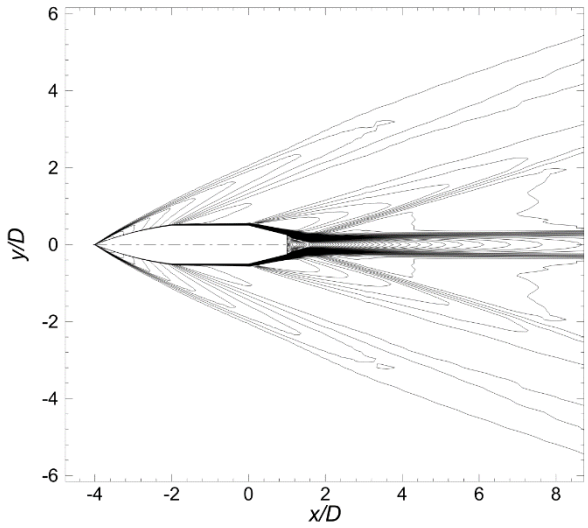

Fig. 8. Mach numer countor around the model at β = 14° and M = 3.0

3.3 Drag of the model

Figure 9 shows drag of the boattail model of 7° for different Mach number. Clearly, the drag at subsonic flow is nearly constant. It becomes large at transonic flow and reduces with Mach number at supersonic conditions. As shown in validation part, the current results show high consistent to previous experimental study. Additionally, numerical methods allow to extend study at subsonic conditions.

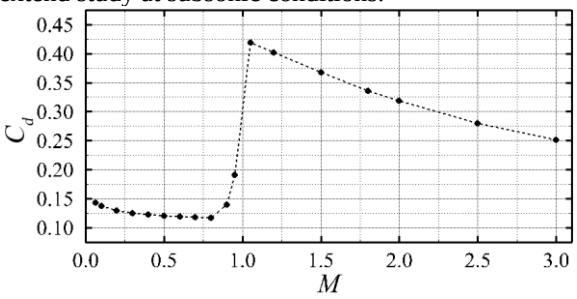

Fig. 9. Drag as a function of Mach number for β = 7°

3.4 Skin-friction topology

To determining flow behavior on the boattail surface, streamwise skin-friction on the surface is analyzed. As shown in previous study by Tran et al.[14], the flow is fully attached on the boattail surfare for the model with angle bellow 12°. Consequently, only boattail model of 14° is analyzed in this step. Figure shows streamwise skin-friction distribution on boattail surface. The region of separation is feature by negative skin-friction values. As can be seen, the separation bubble is formed for M = 0.1. At higher Mach number, flow on boattail surface is smooth and no separation flow is observed. Clearly, the kinetic energy increases with free-stream Mach number. Consequently, the air can move further on the surface and separation flow is delayed. Similar feature is observed for supersonic flow. Consequently, the formation of shock wave is the main factor, which leads to change pressure distribution around after body and increasing drag of the model. The analyzing of shock wave structure is important for explaining drag trend of the model.

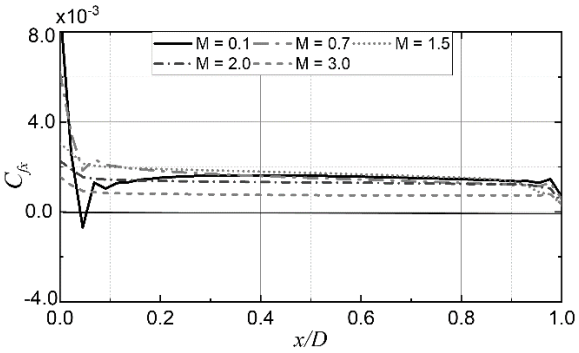

Fig. 10. Distribution of streamwise skin-friction on the boattail surface

3.5 Flow around the models

Figure 11 shows contour of Mach number around the base for boattail model of 7°. The free stream Mach number is 1.5 and 3 in those cases. Clear structure of shock wave is observered. In fact, shock wave occurs around the shoulder and in wave region for both case. Interestingly, as the Mach number increases, the shock wave angle with respect to the *x*-axis decreases. In the reattachment region, shock wave is mixed with near-wake structure to make flow becomes compicated.

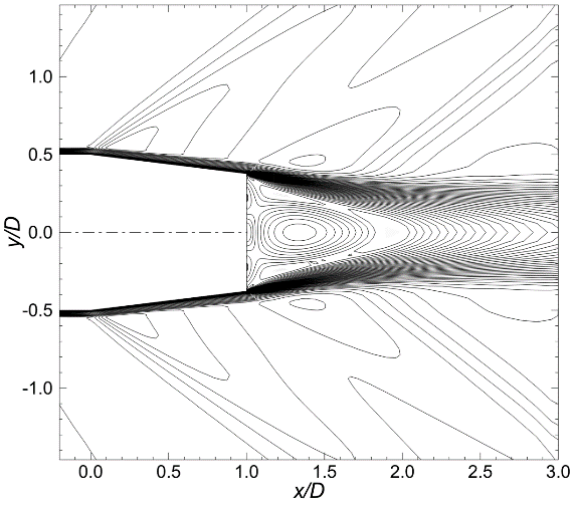

a. M = 1.0

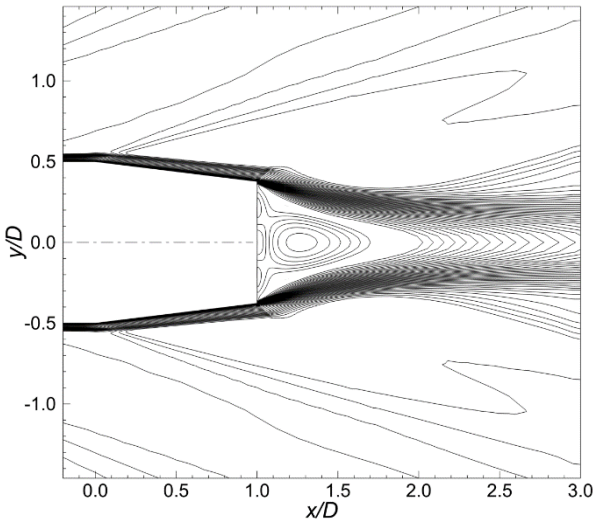

b. M = 3.0

Fig. 11. Countor of Mach number at β = 7° and M = 1.0 (top) and M = 3.0 (bottom)

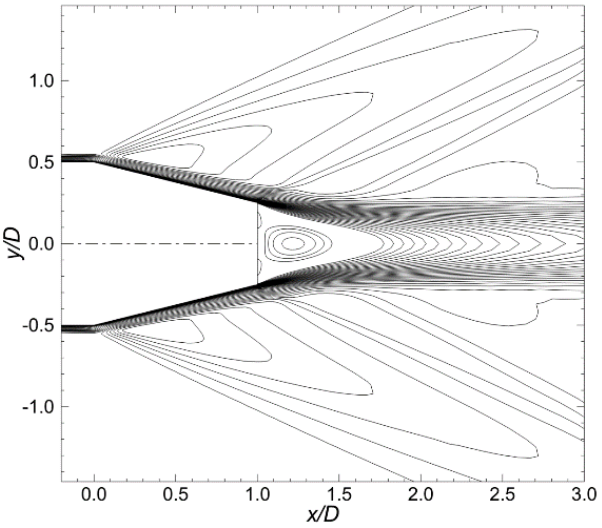

a. M = 1.0

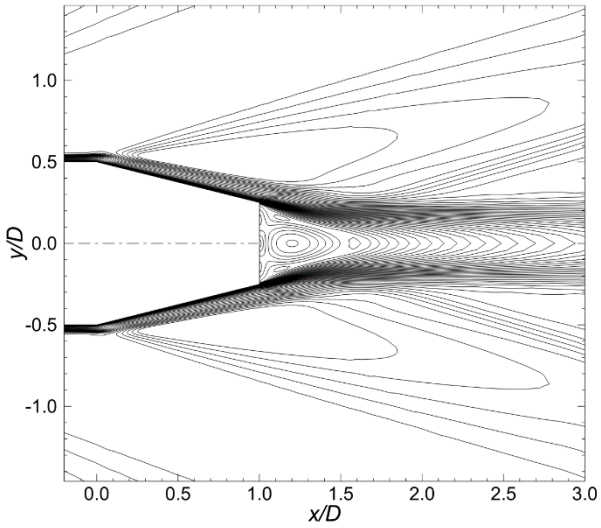

b. M = 3.0

Fig. 12. Countor of Mach number at β = 14° and M = 1.0 (top) and M = 3.0 (bottom)

At boattail angle of 14°, similar structure of shock wave is observed. However, the region of shock wave near the shoulder is expanded and the shock wave in reattachment region moves close to the base. By comparison to the case of 7°, the wake region of the model with angle of 14° becomes smaller.

4 Conclusions

Flow around boattail surface and aerodynamic characteristics of axisymmetric boattail models were studied in wide range of Mach number. RANS *k-ω* turbulence model was selected for averaged flow behavior. The numerical methods showed high ability in analyzing flow behavior and drag trend of the model. Numerical results indicated that drag of the model is nearly constant at subsonic conditions. The increasing Mach number leads to increasing pressure gradient at subsonic conditions. At supersonic flow, pressure distribution on boattail surface is nearly flat, which results in increasing drag. Skin-friction analysis indicated that a separation is formed for low Mach number and it disappears at high free-stream conditions. Shock waves are formed on the shoulder and reattachment region, which leads to flat of pressure distribution on the boattail surface.

Acknowledgments

References

[1] P. R. Viswanath, “Flow management techniques for base and afterbody drag reduction,” *Prog. Aerosp. Sci.*, vol. 32, no. 2–3, pp. 79–129, 1996, doi: 10.1016/0376-0421(95)00003-8.

[2] K. S. Jagtap, K. Sundarraj, N. Kumar, S. Rajnarasimha, and P. S. Kulkarni, “Numerical Study of Base Drag Reduction Using Locked Vortex Flow Management Technique for Lower Subsonic Regime,” *Int. J. Mech. Mechatronics Eng.*, vol. 12, no. 2, pp. 188–191, 2018, doi:

10.5281/zenodo.1316596.

[3] W. A. Mair, "[13] Reduction of base drag by boat-tailed afterbodies in low speed flow.pdf," *Aeronaut. Q.*, vol. 20, pp. 307–320, 1969.

[4] T. H. Tran, T. Ambo, T. Lee, L. Chen, T. Nonomura, and K. Asai, "Effect of boattail angles on the flow pattern on an axisymmetric afterbody surface at low speed," *Exp. Therm. Fluid Sci.*, vol. 99, pp. 324–335, 2018, doi: 10.1016/j.expthermflusci.2018.07.034.

[5] T. H. Tran, T. Ambo, L. Chen, T. Nonomura, and K. Asai, "Effect of boattail angle on pressure distribution and drag of axisymmetric afterbodies under low-speed conditions," *Trans. Jpn. Soc. Aeronaut. Space Sci.*, vol. 62, no. 4, pp. 219–226, 2019, doi: 10.2322/tjsass.62.219.

[6] A. S. Platou, "Improved projectile boattail," *J. Spacecr. Rockets*, vol. 12, no. 12, pp. 727–732, 1975, doi: 10.2514/3.57040.

[7] N. B. Mathur and P. R. Viswanath, "Drag reduction from square base afterbodies at high speeds," *J. Aircr.*, vol. 41, no. 4, pp. 811–820, 2004.

[8] R. Kumar, P. R. Viswanath, and A. Prabhu, "Mean and fluctuating pressure field in boat-tail separated flows at transonic speeds," *39th Aerosp. Sci. Meet. Exhib.*, no. January, 2001, doi: 10.2514/6.2001-582.

[9] T. H. Tran *et al.*, "Effect of Reynolds number on flow behavior and pressure drag of axisymmetric conical boattails at low speeds," *Exp. Fluids*, vol. 60, no. 3, pp. 1–19, 2019, doi: 10.1007/s00348-019-2680-y.

[10] E. Elawwad, A. Ibrahim, A. Elshabkaa, and A. Riad, "Flow computations past a triangular boattailed projectile," *Def. Technol.*, vol. 16, no. 3, pp. 712–719, 2020, doi: 10.1016/j.dt.2019.08.009.

[11] T. H. Tran, H. Q. Dinh, H. Q. Chu, V. Q. Duong, C. Pham, and V. M. Do, "Effect of boattail angle on near-wake flow and drag of axisymmetric models: a numerical approach," *J. Mech. Sci. Technol.*, vol. 35, no. 2, pp. 563–573, Feb. 2021, doi: 10.1007/s12206-021-0115-1.

[12] W. Jiajan, R. S. M. Chue, T. Nguyen, and S. C. M. Yu, "Boattail juncture shaping for spin-stabilized rounds in supersonic flight," *Shock Waves*, vol. 25, no. 2, pp. 189–204, 2015, doi: 10.1007/s00193-015-0550-y.

[13] F. R. Menter, "Two-equation eddy-viscosity turbulence models for engineering applications," *AIAA J.*, vol. 32, no. 8, pp. 1598–1605, 1994.

[14] T. H. Tran *et al.*, "Effect of Reynolds number on flow behavior and pressure drag of axisymmetric conical boattails at low speeds," *Exp. Fluids*, vol. 60, no. 3, pp. 1–21, 2019, doi: 10.1007/s00348-019-2680-y.